AIMS Mathematics, 11(11): 36379–36408.
DOI: 10.3934/math.20261408
Received: 03 August 2026
Revised: 13 October 2026
Accepted: 19 October 2026
Published: 04 November 2026

https://www.aimspress.com/journal/Math

Research article

A dynamic SIR epidemic model with the Taylor collocation method: Analysis of transmission dynamics under intervention changes

Serpil Ünal[1], **Elçin Çelik**[2,*] **and Deniz Uçar**[1]

[1] Department of Mathematics, Faculty of Arts and Sciences, Uşak University 1 Eylul Campus, Uşak, 64200, Türkiye

[2] Department of Mathematics, Faculty of Science, İzmir Institute of Technology, İzmir, 35430, Türkiye

* **Correspondence:** Email: elcincelik@iyte.edu.tr.

Abstract: This study aims to investigate temporal changes in the transmission dynamics of the COVID-19 epidemic and to examine how these changes are associated with government intervention periods. For this purpose, a normalized dynamic SIR model is considered in which the recovery rate, γ, is set to $1/14$ day^{-1} in the primary analysis, while the transmission rate, β, is allowed to vary across the periods identified in the analysis rather than being assumed constant. Changes in the case series are identified using change-point analysis, and the resulting model is solved using the Taylor collocation method. The estimated transmission rates are compared across the full-closure, partial-closure, and gradual-normalization periods using non-parametric statistical methods. The Kruskal–Wallis test revealed a statistically significant overall difference in the estimated transmission rates among the three intervention groups ($H(2) = 14.353$, $p = 0.001$). Subsequent pairwise comparisons using Dunn's post-hoc test with Bonferroni correction indicated significant differences between the full-closure and partial-closure periods and between the full-closure and gradual-normalization periods, whereas the difference between the partial-closure and gradual-normalization periods was not statistically significant. Sensitivity analyses using alternative recovery-rate assumptions ($\gamma = 1/10$ and $\gamma = 1/20$) yielded the same inferential pattern. These findings indicate that the estimated transmission rates varied across the intervention periods and illustrate the potential of the proposed dynamic SIR framework for characterizing temporal transmission patterns under changing intervention conditions.

Keywords: SIR model; change-point analysis; Kruskal–Wallis test; Dunn's test; Taylor collocation method; COVID-19
Mathematics Subject Classification: 34A34, 62F40, 62G10, 65H10, 92D25, 92D30

1. Introduction

Epidemics have posed a persistent threat to public health throughout human history, with consequences extending beyond human health to social and economic systems. Understanding the emergence, progression, and transmission of infectious diseases is therefore an important component of epidemiological research. Epidemiology investigates the distribution and determinants of health-related events within populations and provides a scientific basis for developing strategies for disease prevention and control [1]. In this context, a wide range of analytical and computational approaches have been developed to better understand the dynamics of infectious diseases.

Mathematical modeling has become an important tool for describing epidemic processes and investigating their temporal behavior. One of the fundamental contributions to mathematical epidemiology was made by Kermack and McKendrick [2] through the susceptible–infected–removed (SIR) model. The classical SIR framework represents the evolution of an epidemic by means of a system of ordinary differential equations describing transitions among susceptible, infected, and removed individuals [2–4]. Despite its relatively simple structure, the SIR model provides a useful and mathematically tractable framework for investigating the progression of infectious diseases.

A variety of analytical and numerical techniques have been proposed to obtain approximate solutions to epidemic and population-dynamics models. Hoppensteadt [5], Shakeri and Dehghan [6–8], Evans and Raslan [9], Saadatmandi and Dehghan [10], Akinboro [11], and Uçar and Çelik [12] investigated different numerical approaches to population-dynamics problems. Further contributions to mathematical epidemic modeling and related population models have been reported by Shulgin et al. [13], Schuette and Hethcote [14], Daley and Gani [15], Iannelli [16], Rafei et al. [17], Ahmetolan et al. [18], Nguemdjo et al. [19], Postnikov [20], Record and Pershing [21], Barlow and Weinstein [22], and Kudryashov et al. [23, 24]. Collectively, these studies demonstrate the broad applicability of mathematical and numerical methods to the analysis of population and epidemic dynamics.

More recent studies have extended the classical SIR framework by allowing epidemiological parameters, particularly the transmission rate, to vary over time. Such time-varying formulations provide greater flexibility for representing changes in epidemic dynamics associated with evolving population behavior, public-health measures, and other time-dependent conditions. Spannaus et al. [25] incorporated time-varying transmission and reporting rates into SIR and SEIR models for COVID-19, while Buch et al. [26] developed a flexible framework for inferring time-varying transmission rates from epidemic data.

The COVID-19 pandemic further highlighted the need for epidemic models capable of accommodating temporal changes in transmission. Following the emergence of COVID-19 in Wuhan, China, in late 2019, the disease spread rapidly worldwide. Governments subsequently introduced various non-pharmaceutical interventions, including mobility restrictions, school closures, contact-tracing measures, social distancing, curfews, and different levels of lockdown. Since the type and intensity of these measures changed throughout the epidemic, representing the entire epidemic period using a single constant transmission parameter may fail to capture important temporal variations in transmission dynamics.

The classical SIR model has limitations in representing the heterogeneous transmission patterns observed during the COVID-19 pandemic, particularly in a large and diverse population such as Türkiye. Nevertheless, its mathematical tractability provides a useful basis for examining temporal

variations in transmission when model parameters are allowed to change over time. Accordingly, the present study does not attempt to construct a comprehensive epidemiological representation of COVID-19. Instead, a dynamic SIR framework is employed to investigate changes in the estimated transmission rate, β, across periods characterized by different government interventions.

Several studies have considered modified SIR-type models and time-dependent epidemic parameters to better represent the transmission dynamics of COVID-19. Mbuvha and Marwala [27], for example, emphasized that transmission rates may vary over time and investigated change points in relation to government interventions and voluntary social-distancing measures. Other studies have estimated different transmission and recovery rates for distinct phases of the epidemic while considering measures such as school closures and curfews [28]. Similarly, modeling studies of the COVID-19 outbreak in Italy have highlighted the role of restrictive measures in describing changes in epidemic transmission [29]. Beyond classical integer-order formulations, Alshomrani et al. [30] developed a Caputo fractional-order SIR model for COVID-19 and investigated the model under an optimized fractional order. Collectively, these studies illustrate how extensions and adaptations of the classical SIR framework can be used to represent complex and temporally evolving epidemic dynamics.

Motivated by these considerations, the present study considers a normalized dynamic SIR model in which the recovery rate, γ, is set to $1/14$ day^{-1} in the primary analysis, whereas the transmission rate, β, is allowed to vary across the periods identified in the analysis. The resulting system is approximated using the Taylor collocation method [31, 32]. Rather than treating the epidemic as a single period characterized by a constant transmission rate, temporal changes in the case series are identified through change-point analysis. The resulting periods are subsequently examined in relation to government intervention periods classified into three categories: full closure, partial closure, and gradual normalization.

The estimated transmission rates corresponding to these intervention periods are subsequently evaluated using non-parametric statistical procedures. The Kruskal–Wallis test is used to assess whether the distributions of the estimated transmission rates differ significantly across the intervention periods. When a statistically significant overall difference is detected, Dunn's post-hoc procedure with Bonferroni correction is employed to identify the specific pairs of intervention periods exhibiting statistically significant differences. Thus, the statistical analysis is intended to evaluate differences in transmission-rate estimates across intervention periods rather than to establish a direct causal relationship between government interventions and changes in epidemic transmission.

The main contribution of this study lies in integrating a time-varying transmission structure, change-point analysis, the Taylor collocation method, and statistical comparisons of intervention periods within a unified SIR framework. By allowing β to vary according to detected temporal changes, the proposed approach provides a flexible framework for examining how estimated epidemic transmission patterns differ across changing intervention conditions. The numerical performance of the Taylor collocation approximation is also evaluated through comparison with a high-accuracy reference ODE solver, residual analysis, convergence with respect to the polynomial degree, population-conservation error, and computational cost. In addition, the use of statistical comparisons provides quantitative evidence regarding differences among the identified intervention periods while avoiding causal interpretations that cannot be established solely from the observational data considered in this study.

2. Methodology

This section presents the methods used to model COVID-19 transmission dynamics and to compare the estimated transmission rates across government intervention periods. The methodology consists of the dynamic SIR model, change-point analysis, the Kruskal–Wallis test, and Dunn's post-hoc test.

2.1. SIR model

2.1.1. SIR model for COVID-19

The SIR model is a classical compartmental model used to describe the transmission dynamics of infectious diseases. Originally introduced by Kermack and McKendrick in 1927 [2], the model divides the population into three compartments:

- **Susceptible individuals** ($S(t)$): individuals who are susceptible to infection at time t.
- **Infected individuals** ($I(t)$): individuals who are infected and capable of contributing to disease transmission at time t.
- **Recovered individuals** ($R(t)$): individuals who have recovered from infection and are no longer included in the infected compartment at time t.

Let N denote the total population. Under the assumptions of the model, the population size remains constant and satisfies

$$N = S(t) + I(t) + R(t).$$

For the numerical formulation used in the present study, the compartment variables are expressed as proportions of the total population. Accordingly, we define

$$s(t) = \frac{S(t)}{N}, \qquad i(t) = \frac{I(t)}{N}, \qquad r(t) = \frac{R(t)}{N},$$

where N denotes the constant total population. Hence,

$$s(t) + i(t) + r(t) = 1.$$

This normalization expresses the compartment dynamics in terms of population proportions, with the transmission term written as $\beta s(t)i(t)$ and β interpreted as a rate parameter with units of day^{-1}.

The SIR model considered in this study is based on the following assumptions:

- The total population is assumed to remain constant during the modeled period; therefore, natural births and deaths are not explicitly incorporated into the model.
- For a sufficiently large population, the compartment variables are treated as continuous variables.
- Individuals are assumed to mix homogeneously, so that contact opportunities are not explicitly differentiated among individuals.
- Individuals who are not infected or recovered are considered susceptible to infection.
- Demographic and risk-related heterogeneity, including differences associated with age, sex, social characteristics, and individual contact patterns, is not explicitly represented in the model.

These simplifying assumptions are inherent to the SIR framework used in the present study and are considered when interpreting the model results.

The compartmental transition structure of the SIR model used for COVID-19 is represented as follows:

$$\underset{(S)}{\text{Susceptible}} \xrightarrow{\beta} \underset{(I)}{\text{Infected}} \xrightarrow{\gamma} \underset{(R)}{\text{Recovered}}. \tag{2.1}$$

Here, β denotes the transmission-rate parameter and γ denotes the recovery-rate parameter.

Using the normalized state variables, the corresponding transition rates are represented by

$$(S) \xrightarrow{\beta si} (I) \xrightarrow{\gamma i} (R). \tag{2.2}$$

Accordingly, the normalized SIR model considered in this study is expressed as

$$s'(t) = -\beta(t)s(t)i(t), \tag{2.3}$$

$$i'(t) = \beta(t)s(t)i(t) - \gamma i(t), \tag{2.4}$$

$$r'(t) = \gamma i(t), \tag{2.5}$$

subject to the initial conditions

$$s(t_0) > 0, \qquad i(t_0) > 0, \qquad r(t_0) \geq 0,$$

with

$$s(t_0) + i(t_0) + r(t_0) = 1.$$

Summing the three differential equations gives

$$\frac{d}{dt}\left[s(t) + i(t) + r(t)\right] = 0.$$

Therefore, if

$$s(t_0) + i(t_0) + r(t_0) = 1,$$

then

$$s(t) + i(t) + r(t) = 1$$

for all t in the modeled interval. The numerical conservation error associated with this identity is further examined in the numerical validation analysis.

2.1.2. Method of solution for the SIR model

In this section, a Taylor collocation approximation is constructed for the nonlinear SIR system in Eqs (2.3)–(2.5) by representing each state variable with a truncated Taylor polynomial of degree M [31, 32]. For notational simplicity in the Taylor collocation derivation, the symbols $S(t)$, $I(t)$, and $R(t)$ are retained to denote the corresponding normalized state variables $s(t)$, $i(t)$, and $r(t)$, respectively. Within each identified time segment, the transmission-rate parameter β is treated as constant; therefore, β is written without explicit time dependence in the Taylor collocation derivation below.

$$S(t) = \sum_{n=0}^{M} S_n t^n, \qquad S_n = \frac{S^{(n)}(0)}{n!}, \qquad n = 0, 1, \ldots, M, \qquad 0 \leq t \leq b, \tag{2.6}$$

$$I(t) = \sum_{n=0}^{M} I_n t^n, \qquad I_n = \frac{I^{(n)}(0)}{n!}, \qquad n = 0, 1, \ldots, M, \qquad 0 \le t \le b, \tag{2.7}$$

$$R(t) = \sum_{n=0}^{M} R_n t^n, \qquad R_n = \frac{R^{(n)}(0)}{n!}, \qquad n = 0, 1, \ldots, M, \qquad 0 \le t \le b. \tag{2.8}$$

The truncated Taylor expansions in Eqs (2.6)–(2.8) can be expressed in matrix form as

$$S(t) = T(t)S, \tag{2.9}$$

$$I(t) = T(t)I, \tag{2.10}$$

$$R(t) = T(t)R, \tag{2.11}$$

where

$$T(t) = \begin{bmatrix} 1 & t & t^2 & \cdots & t^M \end{bmatrix} \in \mathbb{R}^{1\times(M+1)},$$

and

$$S = \begin{bmatrix} S_0 \\ S_1 \\ \vdots \\ S_M \end{bmatrix}, \qquad I = \begin{bmatrix} I_0 \\ I_1 \\ \vdots \\ I_M \end{bmatrix}, \qquad R = \begin{bmatrix} R_0 \\ R_1 \\ \vdots \\ R_M \end{bmatrix} \in \mathbb{R}^{(M+1)\times 1}.$$

Here, $T(t)$ denotes the Taylor basis row vector, whereas S, I, and R are the corresponding vectors of unknown Taylor coefficients.

Differentiating the approximations in Eqs (2.6)–(2.8) and expressing the resulting derivatives in matrix form yields

$$S'(t) = T(t)BS, \tag{2.12}$$

$$I'(t) = T(t)BI, \tag{2.13}$$

$$R'(t) = T(t)BR, \tag{2.14}$$

where

$$B = \begin{bmatrix} 0 & 1 & 0 & \cdots & 0 \\ 0 & 0 & 2 & \cdots & 0 \\ \vdots & \vdots & \ddots & \ddots & \vdots \\ 0 & 0 & \cdots & 0 & M \\ 0 & 0 & \cdots & 0 & 0 \end{bmatrix} \in \mathbb{R}^{(M+1)\times(M+1)}$$

is the operational differentiation matrix associated with the Taylor basis. Its entries are defined by

$$B_{ij} = \begin{cases} j, & j = i + 1, \\ 0, & \text{otherwise}, \end{cases} \qquad i, j = 0, 1, \ldots, M.$$

Thus, $T'(t) = T(t)B$, which leads directly to the derivative representations in Eqs (2.12)–(2.14).

The nonlinear product $S(t)I(t)$ appearing in Eq (2.3) can be expressed in matrix form as

$$S(t)I(t) = T(t)T^*(t)\bar{S}, \tag{2.15}$$

where

$$T^*(t) = \begin{bmatrix} T(t) & 0 & \cdots & 0 \\ 0 & T(t) & \cdots & 0 \\ \vdots & \vdots & \ddots & \vdots \\ 0 & 0 & \cdots & T(t) \end{bmatrix} \in \mathbb{R}^{(M+1)\times(M+1)^2}$$

is the block-diagonal matrix formed by $M+1$ copies of the Taylor basis vector $T(t)$, and

$$\bar{S} = \begin{bmatrix} S_0 I \\ S_1 I \\ \vdots \\ S_M I \end{bmatrix} \in \mathbb{R}^{(M+1)^2\times 1},$$

with

$$I = \begin{bmatrix} I_0 & I_1 & \cdots & I_M \end{bmatrix}^T.$$

Thus, $\bar{S}$ collects the coefficient products required to represent the nonlinear term $S(t)I(t)$.

By substituting the matrix representations above into the SIR system in Eqs (2.3)–(2.5), the following equations are obtained:

$$T(t)BS + \beta T(t)T^*(t)\bar{S} = 0, \tag{2.16}$$

$$\left[T(t)B + \gamma T(t)\right] I - \beta T(t)T^*(t)\bar{S} = 0, \tag{2.17}$$

$$T(t)BR - \gamma T(t)I = 0. \tag{2.18}$$

For compactness, the first two equations of the SIR system can be rewritten as

$$D_1(t)S + H_1(t)\bar{S} = 0, \tag{2.19}$$

$$D_2(t)I + H_2(t)\bar{S} = 0, \tag{2.20}$$

where

$$D_1(t) = T(t)B, \qquad H_1(t) = \beta T(t)T^*(t),$$

and

$$D_2(t) = T(t)B + \gamma T(t), \qquad H_2(t) = -\beta T(t)T^*(t).$$

Define the block matrices

$$D(t) = \begin{bmatrix} D_1(t) & 0 \\ 0 & D_2(t) \end{bmatrix}, \qquad H(t) = \begin{bmatrix} H_1(t) & 0 \\ 0 & H_2(t) \end{bmatrix},$$

together with

$$\overline{SI} = \begin{bmatrix} S \\ I \end{bmatrix} \in \mathbb{R}^{2(M+1)\times 1},$$

$$\overline{\overline{S}} = \begin{bmatrix} \bar{S} \\ \bar{S} \end{bmatrix} \in \mathbb{R}^{2(M+1)^2\times 1},$$

and

$$G(t) = \begin{bmatrix} 0 \\ 0 \end{bmatrix} \in \mathbb{R}^{2\times 1}.$$

Equations (2.19) and (2.20) can be written in compact form as

$$D(t)\overline{SI} + H(t)\overline{\overline{S}} = G(t). \tag{2.21}$$

The collocation points are chosen as the equally spaced nodes

$$t_s = \frac{b}{M}s, \qquad s = 0, 1, \ldots, M, \tag{2.22}$$

over the interval $[0, b]$. Thus, a Taylor approximation of degree M is associated with $M + 1$ equally spaced collocation points $t_0, t_1, \ldots, t_M$. At each collocation point $t = t_s$, the matrices $D(t_s)$ and $H(t_s)$ are completely determined, whereas the Taylor coefficient vectors remain unknown. Since products of the unknown Taylor coefficients are involved through the nonlinear term $S(t)I(t)$, the resulting algebraic system is nonlinear.

By enforcing Eq (2.21) at each collocation point t_s, we obtain

$$D(t_s)\overline{SI} + H(t_s)\overline{\overline{S}} = G(t_s), \qquad s = 0, 1, \ldots, M. \tag{2.23}$$

Evaluating the two equations in Eq (2.21) at each of the $M + 1$ collocation points therefore provides $2(M + 1)$ scalar equations. Equivalently, the collocation equations can be expressed in global matrix form as

$$\bar{D}\,\overline{SI} + \bar{H}\,\overline{\overline{S}} = \bar{G}, \tag{2.24}$$

where

$$\bar{D} = \begin{bmatrix} D(t_0) \\ D(t_1) \\ \vdots \\ D(t_M) \end{bmatrix} \in \mathbb{R}^{2(M+1)\times 2(M+1)},$$

$$\bar{H} = \begin{bmatrix} H(t_0) \\ H(t_1) \\ \vdots \\ H(t_M) \end{bmatrix} \in \mathbb{R}^{2(M+1)\times 2(M+1)^2},$$

and

$$\bar{G} = \begin{bmatrix} G(t_0) \\ G(t_1) \\ \vdots \\ G(t_M) \end{bmatrix} \in \mathbb{R}^{2(M+1)\times 1}.$$

The initial conditions for the susceptible and infected state variables are expressed in matrix form as

$$T(0)S = \lambda_1, \tag{2.25}$$

$$T(0)I = \lambda_2. \tag{2.26}$$

The initial conditions in Eqs (2.25) and (2.26) are imposed by replacing the corresponding two equations in the collocation system. Consequently, the collocation procedure yields a nonlinear algebraic system consisting of $2(M + 1)$ equations for the $2(M + 1)$ unknown Taylor coefficients contained in S and I. After solving this nonlinear system, the approximate solutions $S(t)$ and $I(t)$ are obtained by substituting the computed coefficients into their corresponding truncated Taylor representations.

Once $I(t)$ has been determined, the recovered state variable $R(t)$ is obtained from the third equation of the SIR system,

$$R'(t) = \gamma I(t),$$

together with the initial condition

$$R(0) = R_0.$$

Thus, $R(t)$ can be recovered after solving the nonlinear algebraic system for the Taylor coefficients of $S(t)$ and $I(t)$. Since $R(t)$ is reconstructed by integrating the relation $R'(t) = \gamma I(t)$, its polynomial representation may be one degree higher than that used for $S(t)$ and $I(t)$.

Although standard numerical ODE solvers can also be employed for SIR-type systems, the Taylor collocation approach provides a polynomial representation of the state variables within a matrix-based framework. This formulation converts the differential system into a finite-dimensional nonlinear algebraic system for the Taylor coefficients and facilitates the direct incorporation of model parameters into the approximation. In the present study, this framework is used to obtain approximate solutions of the SIR system for the specified model parameters and to facilitate the subsequent numerical evaluation of the model dynamics.

2.1.3. Numerical validation and convergence analysis

To assess the numerical accuracy and computational behavior of the Taylor collocation method, an independent validation problem was considered before its application to the epidemiological analysis. This validation is intended solely to evaluate the numerical implementation of the Taylor collocation scheme and is independent of the transmission-rate estimation procedure used in the application.

For the validation problem, the total population was taken as

$$N = 82{,}000{,}000,$$

and the normalized initial conditions were specified as

$$s(0) = 1 - \frac{1}{N}, \qquad i(0) = \frac{1}{N}, \qquad r(0) = 0.$$

The recovery-rate parameter was set to

$$\gamma = \frac{1}{14},$$

and a prescribed time-dependent transmission rate was used:

$$\beta(t) = 0.027269 \exp(-0.002547133109t).$$

The validation was performed over the interval

$$0 \le t \le 1.$$

For the degree-3 Taylor approximation ($M = 3$), the nominal collocation nodes were

$$t_0 = 0, \qquad t_1 = \frac{1}{3}, \qquad t_2 = \frac{2}{3}, \qquad t_3 = 1.$$

In forming the square nonlinear algebraic system, the two differential-equation conditions associated with the final collocation node were replaced by the two initial conditions. Consequently, the susceptible and infected differential equations were enforced at $t = 0$, $1/3$, and $2/3$, yielding six collocation equations together with two initial-condition equations for the eight unknown Taylor coefficients.

The numerical solution obtained with the Taylor collocation method was compared with a high-accuracy Runge–Kutta–Fehlberg (RKF45) numerical reference solution. Both the absolute and relative tolerances of the RKF45 solver were set to 10^{-12}. The comparison was performed at 101 equally spaced points over the interval $[0, 1]$. The root-mean-square error (RMSE), mean absolute error (MAE), and maximum absolute error were calculated for the normalized susceptible, infected, and recovered state variables. The results for $M = 3$ are presented in Table 1.

Table 1. Comparison of the degree-3 Taylor collocation solution with the RKF45 reference solution.

State variable	RMSE	MAE	Maximum absolute error
$s(t)$	3.862×10^{-16}	3.015×10^{-16}	7.142×10^{-16}
$i(t)$	3.931×10^{-16}	3.061×10^{-16}	7.341×10^{-16}
$r(t)$	8.162×10^{-16}	6.345×10^{-16}	1.645×10^{-15}

The results indicate very close numerical agreement between the Taylor collocation approximation and the RKF45 reference solution for this test configuration, with discrepancies on the order of 10^{-15} or smaller.

In addition to the comparison with the reference solution, the residuals of the normalized SIR equations were evaluated. The residual functions were defined as

$$\mathcal{R}_s(t) = s_T'(t) + \beta(t) s_T(t) i_T(t), \tag{2.27}$$

$$\mathcal{R}_i(t) = i_T'(t) - \beta(t) s_T(t) i_T(t) + \gamma i_T(t), \tag{2.28}$$

$$\mathcal{R}_r(t) = r_T'(t) - \gamma i_T(t), \tag{2.29}$$

where $s_T(t)$, $i_T(t)$, and $r_T(t)$ denote the Taylor approximations. The RMSE and maximum absolute residuals evaluated over the same 101 points are reported in Table 2.

The very small residual associated with the recovered compartment results from the fact that $r_T(t)$ is reconstructed by direct integration of the relation $r'(t) = \gamma i(t)$ after the approximation for $i(t)$ has been obtained.

Table 2. Residual errors of the degree-3 Taylor collocation approximation.

Residual	RMSE	Maximum absolute residual
$\mathcal{R}_s$	2.237×10^{-16}	7.883×10^{-16}
$\mathcal{R}_i$	2.221×10^{-16}	7.831×10^{-16}
$\mathcal{R}_r$	2.310×10^{-39}	6.000×10^{-39}

To examine convergence with respect to the polynomial degree, the numerical experiment was repeated using $M = 2$, $M = 3$, and $M = 4$. The corresponding RMSE and maximum absolute errors relative to the RKF45 reference solution are summarized in Table 3.

Table 3. Convergence of the Taylor collocation approximation with respect to the polynomial degree.

M	State variable	RMSE	Maximum absolute error
2	$s(t)$	7.139×10^{-15}	2.396×10^{-14}
2	$i(t)$	8.183×10^{-15}	2.746×10^{-14}
2	$r(t)$	9.128×10^{-16}	1.640×10^{-15}
3	$s(t)$	3.862×10^{-16}	7.142×10^{-16}
3	$i(t)$	3.931×10^{-16}	7.341×10^{-16}
3	$r(t)$	8.162×10^{-16}	1.645×10^{-15}
4	$s(t)$	4.046×10^{-16}	8.126×10^{-16}
4	$i(t)$	4.113×10^{-16}	8.316×10^{-16}
4	$r(t)$	8.159×10^{-16}	1.644×10^{-15}

A substantial reduction in the numerical error is observed when the polynomial degree is increased from $M = 2$ to $M = 3$. Increasing the degree further to $M = 4$ does not produce a meaningful additional reduction in the error for this validation problem. These results indicate that $M = 3$ provides sufficient numerical accuracy for the present test configuration while maintaining a relatively low polynomial degree.

The population-conservation property was also examined numerically. For the normalized system, the conservation error was defined as

$$E(t) = |s(t) + i(t) + r(t) - 1| .$$

The corresponding RMSE and maximum conservation errors for the degree-3 Taylor approximation and the RKF45 reference solution are given in Table 4.

Table 4. Population-conservation errors for the Taylor collocation and RKF45 solutions.

Method	RMSE	Maximum error
Taylor collocation ($M = 3$)	4.878×10^{-17}	1.964×10^{-16}
RKF45	7.870×10^{-30}	3.000×10^{-29}

Both numerical approaches therefore preserve the normalized population constraint with very small numerical error over the validation interval.

Finally, the computational cost of the two numerical approaches was examined using mean computational times obtained over 100 runs. The construction time and the time required to evaluate the resulting solution at 101 points are reported in Table 5.

Table 5. Mean computational times over 100 runs for the Taylor collocation and RKF45 approaches.

Method	Construction time (s)	Evaluation time (s)
Taylor collocation ($M = 3$)	0.00507	0.00101
RKF45	0.00130	0.00460

The computational results do not indicate that the Taylor collocation method is universally faster than a standard numerical ODE solver. In this validation problem, RKF45 required less time for the initial construction of the numerical solution, whereas evaluation of the explicit Taylor polynomial at the 101 prescribed points required less time. The principal practical advantage of the Taylor collocation formulation is therefore its explicit polynomial representation, which permits repeated evaluation, differentiation, integration, and residual calculation without repeated time-stepping. Together with the reference-solution comparison, residual analysis, convergence assessment, and population-conservation results, these findings provide numerical support for the implementation of the Taylor collocation method used in this study.

2.2. Change-point analysis (CPA)

Change-point analysis (CPA) is a statistical approach used to detect structural changes in sequential or time-series data and to identify the locations at which such changes occur. Change-point methods are particularly useful for examining changes in the behavior of time-dependent data and have been applied in various contexts to investigate temporal heterogeneity [33, 34]. In the present study, the cumulative sum (CUSUM) approach combined with bootstrap resampling is used to identify potential changes in the time series [33].

Let $Y_1, Y_2, \ldots, Y_N$ denote the observed time-series data, and let $\overline{Y}$ denote the sample mean. The cumulative sums are defined by

$$S_0 = 0, \tag{2.30}$$

and

$$S_i = S_{i-1} + \left(Y_i - \overline{Y}\right), \qquad i = 1, 2, \ldots, N. \tag{2.31}$$

Since the deviations from the sample mean sum to zero, $S_N = 0$. The pattern of the CUSUM sequence provides information about possible changes in the underlying data. A sustained positive slope indicates that the observations tend to remain above the overall mean during the corresponding period, whereas a sustained negative slope indicates that they tend to remain below the mean. Therefore, a marked change in the direction of the CUSUM curve may indicate a potential change point. Once a change point is identified, the time series can be divided at that location, and the procedure can be repeated within the resulting segments to identify additional change points [33].

Although the CUSUM curve can be used to identify the location of a potential change, bootstrap resampling is employed to assess the statistical support for the detected change. For the original

sequence, the magnitude of variation in the cumulative sums is calculated as

$$S_{\text{diff}} = S_{\max} - S_{\min}, \tag{2.32}$$

where $S_{\max}$ and $S_{\min}$ denote the maximum and minimum values of the CUSUM sequence, respectively.

Bootstrap samples are then generated by randomly resampling the observations, and a CUSUM sequence together with the corresponding S_{diff} value is calculated for each bootstrap sample. The variation observed in the original time series is subsequently compared with the variations obtained from the bootstrap samples. Let B denote the total number of bootstrap replications and B^* the number of bootstrap samples for which the bootstrap CUSUM difference is smaller than that obtained from the original sequence. The bootstrap confidence level associated with the detected change point is calculated as [33]

$$\text{Confidence level} = \frac{B^*}{B} \times 100\%. \tag{2.33}$$

The bootstrap procedure therefore provides a quantitative assessment of the statistical support for each detected change point. In the present study, a total of 1000 bootstrap replications were performed, and a minimum confidence level of 80% was adopted as the criterion for inclusion of a detected change point. The 80% level is among the alternative inclusion confidence levels specified in the Change-Point Analyzer methodology [35]. Accordingly, change points with bootstrap confidence levels of at least 80% were retained and used to segment the time series for the subsequent analyses.

2.3. Kruskal–Wallis test

The Kruskal–Wallis test is a rank-based non-parametric method used to compare three or more independent groups when the assumptions required for a parametric one-way analysis of variance, particularly the normality assumption, are not satisfied. Rather than relying directly on the original observations, the procedure is based on the ranks assigned to the pooled data. It is therefore suitable for evaluating differences among independent groups when the outcome cannot reasonably be assumed to follow a normal distribution [36, 37].

In the present study, the Kruskal–Wallis test is used to evaluate whether the estimated transmission rates differ across the full-closure, partial-closure, and gradual-normalization periods. The null hypothesis is that the distributions of the estimated transmission rates are the same across the intervention periods, whereas the alternative hypothesis is that at least one intervention period differs from the others. A statistically significant Kruskal–Wallis result indicates an overall difference among the intervention periods but does not identify which specific pairs differ. Therefore, when the null hypothesis is rejected, pairwise comparisons are subsequently performed using Dunn's post-hoc test with Bonferroni correction for multiple comparisons [36].

2.3.1. Dunn's post-hoc test

Following a statistically significant Kruskal–Wallis test, Dunn's post-hoc test is used to determine which pairs of independent groups differ significantly. The procedure is based on differences between the mean ranks of the groups and enables pairwise comparisons following a significant omnibus

test [36]. For groups i and j, the standardized test statistic is calculated as

$$z_{ij} = \frac{\overline{R}_i - \overline{R}_j}{\sqrt{\left[\frac{N(N+1)}{12} - \frac{\sum_k (t_k^3 - t_k)}{12(N-1)}\right]\left(\frac{1}{n_i} + \frac{1}{n_j}\right)}}, \tag{2.34}$$

where $\overline{R}_i$ and $\overline{R}_j$ denote the mean ranks of groups i and j, respectively; n_i and n_j are the corresponding sample sizes; N is the total number of observations; and t_k denotes the number of tied observations in the kth group of tied ranks. When no ties are present, the tie-correction term is zero and the expression reduces to the standard Dunn test statistic.

The resulting z_{ij} statistic is evaluated using the standard normal distribution. To control the family-wise error rate arising from multiple pairwise comparisons, the Bonferroni correction is applied [36, 37]. For m pairwise comparisons, the adjusted significance level is defined as

$$\alpha_{\text{adj}} = \frac{\alpha}{m}. \tag{2.35}$$

In the present study, three intervention periods are compared, resulting in

$$m = \binom{3}{2} = 3.$$

Therefore, for an overall significance level of $\alpha = 0.05$, the Bonferroni-adjusted significance level is

$$\alpha_{\text{adj}} = \frac{0.05}{3} = 0.0167.$$

For the two-sided pairwise comparisons, this adjusted significance level corresponds to an approximate critical value of

$$|z_{ij}| > 2.394.$$

Accordingly, a pairwise difference is considered statistically significant when the Bonferroni-adjusted p-value is less than 0.05, equivalently, when the unadjusted pairwise p-value is less than $\alpha_{\text{adj}} = 0.0167$. The corresponding z statistics, Bonferroni-adjusted p-values, and statistical decisions are reported for each pairwise comparison.

3. Application to COVID-19 data

The analysis was conducted using COVID-19 data obtained from the Ministry of Health of the Republic of Türkiye [38]. The dataset comprises daily newly reported cases and cumulative case counts from the date of the first reported COVID-19 case in Türkiye through November 21, 2021. The analyses were performed using Excel, Maple, and SPSS 15.0.

A normalized dynamic SIR model solved using the Taylor collocation method was employed to characterize the transmission dynamics of COVID-19 during the study period. In the primary analysis, the recovery rate, γ, was set to $1/14$ day^{-1}, whereas the transmission rate, β, was allowed to vary across the periods identified in the analysis. For each intervention segment, the transmission rate was

estimated using a log-linear ordinary least-squares (OLS) procedure. From the infected-state equation of the normalized SIR model,

$$i'(t) = [\beta s(t) - \gamma]\, i(t),$$

it follows that

$$\frac{d}{dt} \ln i(t) = \beta s(t) - \gamma.$$

For the local estimation within each segment, the susceptible proportion was approximated as $s(t) \approx 1$. Under this approximation,

$$\frac{d}{dt} \ln i(t) \approx \beta - \gamma,$$

which provides the local exponential representation used for estimating the segment-specific transmission rate.

Let Y_{ij} denote the daily number of newly reported COVID-19 cases observed at time t_{ij} in segment j, where n_j is the number of observations in that segment. These observed daily case counts are not mathematically identical to the infected-state variable $I(t)$ of the SIR model; rather, they are used as an observational proxy for the local infected-state dynamics. Specifically, daily reported new cases represent an incidence measure, whereas the infected-state variable $I(t)$ in the standard SIR model represents the number of individuals currently in the infectious compartment. Therefore, the use of daily case counts in the segment-wise log-linear regression constitutes an empirical approximation rather than a direct observation of the SIR infected-state variable.

Accordingly, the segment-wise empirical representation is expressed as

$$Y_{ij} \approx I_{0,j} \exp\left[(\beta_j - \gamma) t_{ij}\right],$$

where $I_{0,j}$ serves as a segment-specific scale parameter for the observed daily case series and should not be interpreted as a direct measurement of the initial number of infectious individuals.

Taking the natural logarithm, the corresponding statistical regression model is written as

$$\ln(Y_{ij}) = a_j + b_j t_{ij} + \varepsilon_{ij},$$

where $a_j = \ln(I_{0,j})$ and $b_j = \beta_j - \gamma$. Here, ε_{ij} denotes the regression error term, accounting for deviations of the observed log-transformed case counts from the fitted local linear trend.

For each segment, the coefficients a_j and b_j were obtained by minimizing the ordinary least-squares objective function

$$Q_j(a_j, b_j) = \sum_{i=1}^{n_j} \left[\ln(Y_{ij}) - (a_j + b_j t_{ij})\right]^2.$$

The slope coefficient was calculated directly using the closed-form least-squares expression

$$\widehat{b_j} = \frac{n_j \sum_{i=1}^{n_j} t_{ij} \ln(Y_{ij}) - \left(\sum_{i=1}^{n_j} t_{ij}\right)\left(\sum_{i=1}^{n_j} \ln(Y_{ij})\right)}{n_j \sum_{i=1}^{n_j} t_{ij}^2 - \left(\sum_{i=1}^{n_j} t_{ij}\right)^2},$$

and the corresponding transmission-rate estimate was then obtained as

$$\widehat{\beta_j} = \widehat{b_j} + \gamma,$$

where $\gamma = 1/14$ day^{-1} in the primary analysis.

Because the segment-specific transmission rates were obtained from an unconstrained log-linear OLS estimation, no non-negativity constraint was imposed on $\widehat{\beta}_j$. Consequently, a negative estimate may arise when the estimated local decline in the observed case series is sufficiently steep that $\widehat{b}_j + \gamma < 0$. In the present analysis, this occurred for one segment, yielding $\widehat{\beta} = -0.0200$. Such a value should not be interpreted as a biologically negative transmission rate. Rather, it reflects a limitation of the local unconstrained approximation when applied to a rapidly declining segment of the observed case series. The estimate was retained without truncation to preserve the original estimation procedure and to avoid introducing a post-estimation constraint selectively into the statistical analysis.

The numbers of observations used in the 13 full-closure segments were 10, 8, 13, 8, 7, 7, 10, 7, 18, 22, 7, 8, and 8; those in the 9 partial-closure segments were 9, 7, 7, 8, 16, 8, 10, 13, and 7; and those in the 38 gradual-normalization segments were 10, 14, 25, 10, 14, 8, 21, 10, 25, 10, 14, 9, 8, 12, 13, 8, 11, 10, 6, 6, 4, 5, 7, 9, 8, 10, 13, 19, 10, 5, 8, 11, 19, 15, 21, 20, 20, and 12, respectively.

Since the OLS coefficients were obtained analytically from the closed-form expressions, no iterative nonlinear optimization algorithm, such as the Gauss–Newton or Levenberg–Marquardt method, was employed. Consequently, no numerical convergence or stopping tolerance was required in the estimation procedure. The choice of $\gamma = 1/14$ day^{-1} corresponds to an assumed mean residence/recovery time of 14 days in the infectious compartment and is consistent with values adopted in previous COVID-19 modeling studies.

To evaluate the robustness of the statistical findings to this assumption, a sensitivity analysis was additionally conducted using $\gamma = 1/10$ and $\gamma = 1/20$ day^{-1}, with β re-estimated for the same periods under each recovery-rate specification. The alternative values were selected to represent shorter and longer assumed mean residence/recovery times around the primary 14-day specification and are consistent with recovery-rate values examined in previous COVID-19 studies [39].

During the COVID-19 pandemic, a range of public health measures were implemented in Türkiye, including physical-distancing measures, travel restrictions, quarantine practices, temporary closures of schools and workplaces, and restrictions targeting specific population groups. For the purposes of the present analysis, the intervention periods were classified into three main categories: full closure, partial closure, and gradual normalization, representing different levels of restrictions implemented during the study period. The detected change points were subsequently examined in relation to the government intervention periods presented in Figure 1.

The classification of the estimated transmission-rate segments into the three intervention categories was based on the intervention period in which each segment occurred and was independent of the temporal matching of individual change points to specific intervention dates. For the latter comparison, a predefined temporal window of ± 14 days was used. A detected change point was considered to correspond temporally to a specific government intervention only when the intervention date occurred within 14 days before or after the change-point date. When no intervention date fell within this window, the change point was classified as having no clear corresponding intervention.

To provide a transparent temporal comparison, the exact detected change-point dates, corresponding intervention dates, temporal differences between them, intervention categories, and estimated transmission rates are reported in Supplementary Table S1. These temporal correspondences were used to describe chronological relationships and were not interpreted as evidence of a causal effect of individual government interventions. The timeline of the government interventions considered in the

analysis is presented in Figure 1.

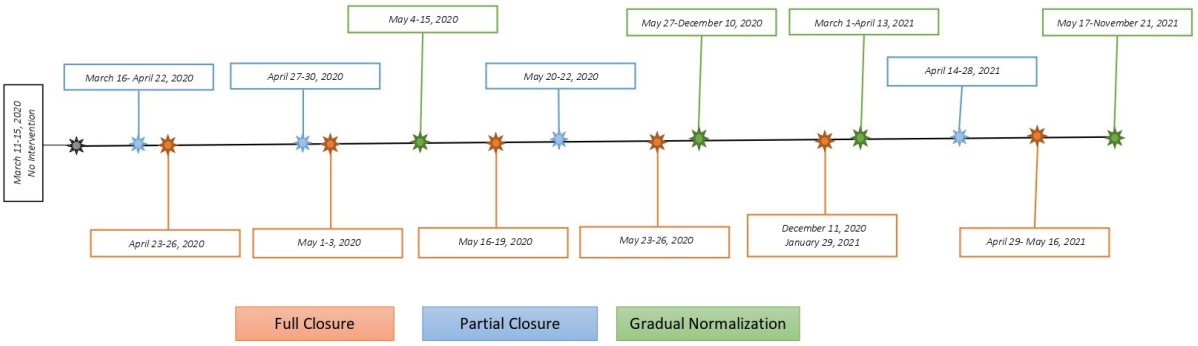


Figure 1. Timeline of the government interventions considered in the study.

Figure 1 presents the timeline of the government interventions considered in the study. To identify potential structural changes in the COVID-19 case series, the CUSUM-based change-point analysis described in Section 2.2 was applied. The resulting CUSUM curve is presented in Figure 2.

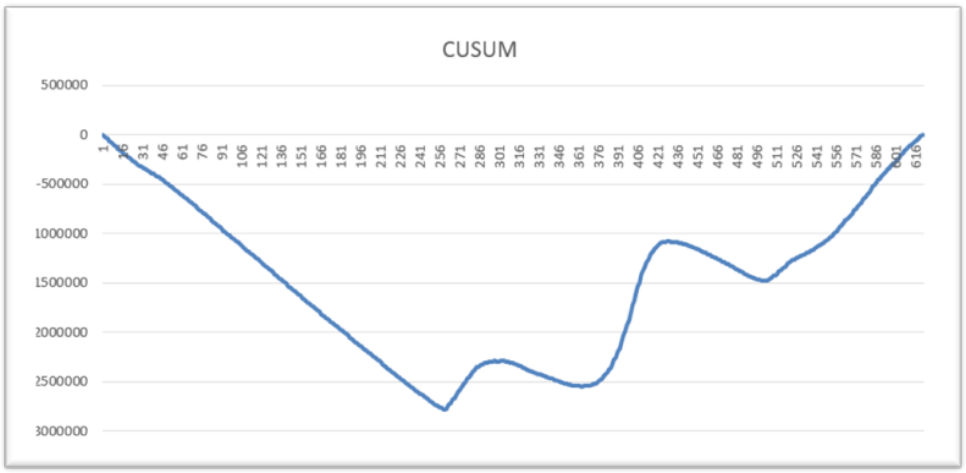


Figure 2. CUSUM chart for the COVID-19 case series.

As shown in Figure 2, the CUSUM curve exhibits a marked change in direction around the 260th day, suggesting a potential structural change in the case series. Prior to this point, the CUSUM curve follows a predominantly downward pattern, whereas an upward pattern is observed thereafter. This change in direction indicates a possible shift in the behavior of the observed case counts. Following the initial CUSUM analysis, the same procedure was applied to the resulting segments to identify additional potential change points.

The statistical support for each detected change point was subsequently assessed using the bootstrap procedure described in Section 2.2. A total of 1000 bootstrap replications were performed, and a minimum bootstrap confidence level of 80% was adopted as the criterion for retaining a detected change point. The 80% level is among the alternative inclusion confidence levels specified in the Change-Point Analyzer methodology [35]. Accordingly, only change points with bootstrap confidence

levels of at least 80% were retained for the subsequent analyses. The retained change points and their corresponding bootstrap confidence levels are presented in Figure 3.

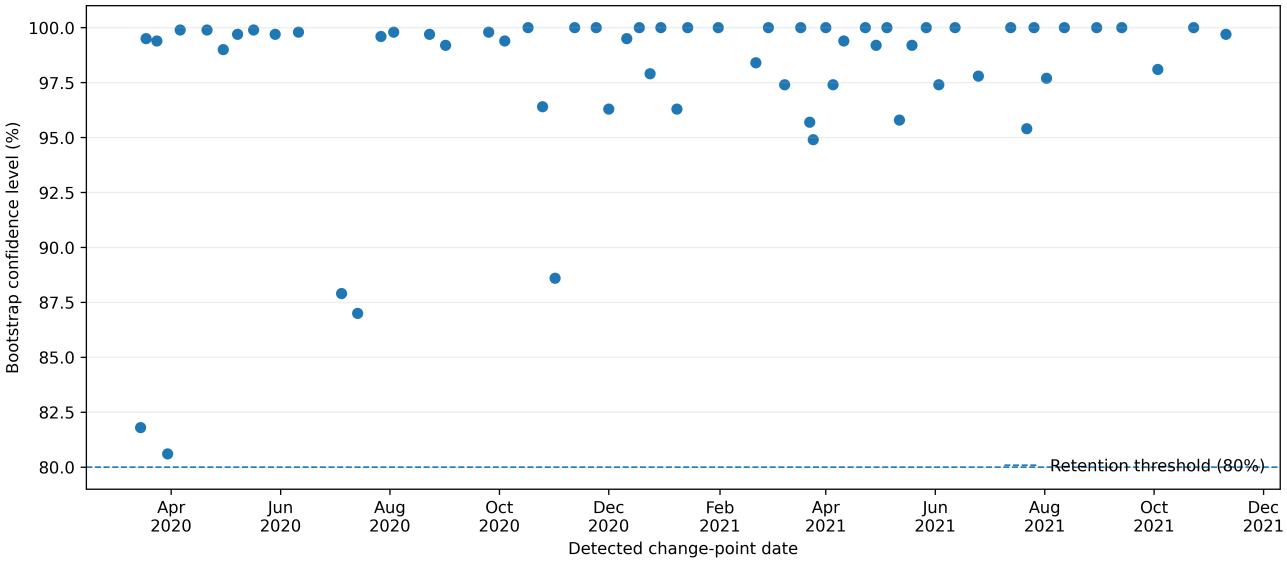


Figure 3. Detected change points and their corresponding bootstrap confidence levels. The dashed horizontal line indicates the 80% bootstrap confidence threshold used as the criterion for retaining detected change points.

Figure 3 summarizes the retained change points throughout the study period, together with their corresponding bootstrap confidence levels. These change points were subsequently examined in relation to the government intervention timeline presented in Figure 1. Specific intervention dates falling within the predefined ±14-day window were considered to correspond temporally to the detected change points, whereas change points for which no intervention occurred within this window were regarded as having no clear corresponding intervention. The detailed temporal relationships, together with the intervention-period classifications and estimated transmission rates, are reported in Supplementary Table S1.

Since the purpose of the study is to examine variation in the transmission rate across different intervention periods, the retained change points were used to define the time intervals for which the transmission parameter β was estimated. For each interval, β was estimated using the log-linear OLS procedure described above. The resulting estimates of β, together with the corresponding intervention categories considered during the study period, are presented in Figure 4.

As illustrated in Figure 4, the estimated transmission rates (β) vary across the intervention periods. Prior to the between-group comparisons, potential serial dependence among the chronologically ordered transmission-rate estimates was assessed using the autocorrelation function (ACF) and the Ljung–Box test. At lag 1, the autocorrelation coefficient was 0.155, and the Ljung–Box test was not statistically significant ($Q(1) = 1.509$, $p = 0.219$). At lag 2, the autocorrelation coefficient was 0.229, and the Ljung–Box test also remained non-significant ($Q(2) = 4.871$, $p = 0.088$). The Ljung–Box tests remained non-significant across the remaining examined lags, providing no evidence of significant serial dependence in the estimated transmission-rate series.

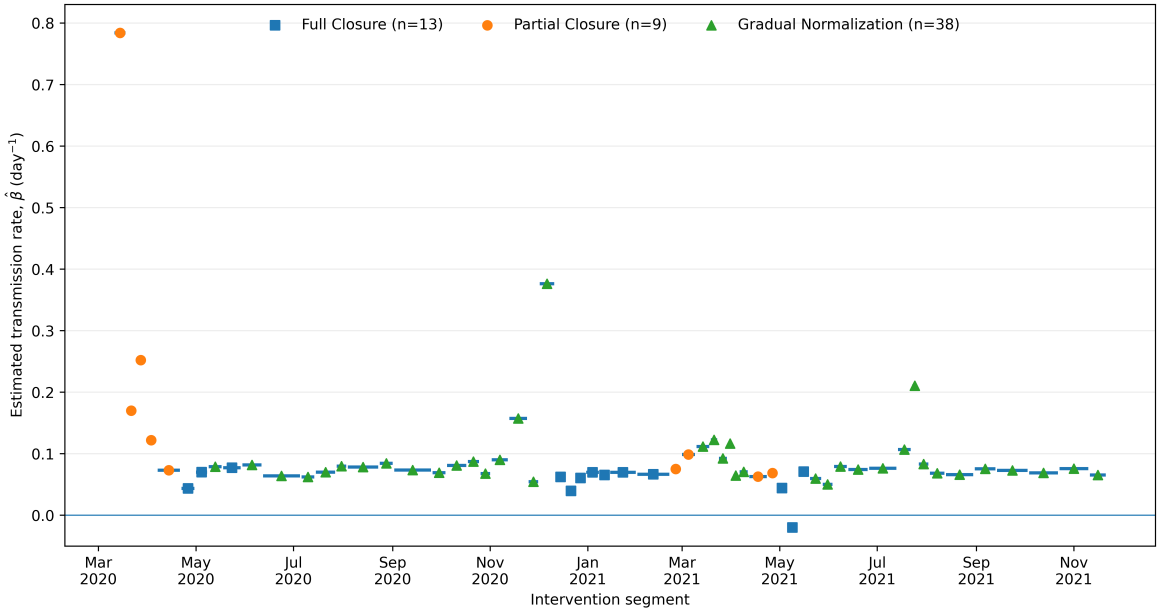


Figure 4. Estimated transmission rates across intervention segments. Horizontal segments indicate the time interval over which each estimated transmission rate was assumed constant.

The distributions of the estimated transmission rates within each intervention period were then assessed for normality using the Kolmogorov–Smirnov and Shapiro–Wilk tests. As shown in Table 6, both tests indicated statistically significant departures from normality within the full-closure ($n = 13$), partial-closure ($n = 9$), and gradual-normalization ($n = 38$) groups. Accordingly, a non-parametric approach was adopted for the subsequent comparison of the intervention groups.

Table 6. Results of the normality tests for the estimated transmission rates.

Intervention period	Kolmogorov–Smirnov			Shapiro–Wilk		
	Statistic	n	p-value	Statistic	n	p-value
Full closure	0.274	13	0.009	0.708	13	0.001
Partial closure	0.289	9	0.029	0.644	9	< 0.001
Gradual normalization	0.307	38	< 0.001	0.519	38	< 0.001

Note: The Kolmogorov–Smirnov test uses the Lilliefors significance correction.

The results of the Kruskal–Wallis test comparing the estimated transmission rates across the intervention groups are presented in Table 7.

Table 7. Results of the Kruskal–Wallis test for the estimated transmission rates.

Test	Test statistic	df	p-value	N
Kruskal–Wallis	14.353	2	0.001	60

The Kruskal–Wallis test indicated a statistically significant overall difference in the estimated transmission rates among the three intervention groups ($H(2) = 14.353$, $p = 0.001$). Thus, the null hypothesis that the distributions of the estimated transmission rates were the same across the intervention groups was rejected. However, the Kruskal–Wallis test does not identify which specific

pairs of groups differ. Therefore, Dunn's post-hoc pairwise comparisons with Bonferroni correction were performed to further examine the differences between the intervention groups.

Dunn's post-hoc pairwise comparisons with Bonferroni correction indicated statistically significant differences between the full-closure and partial-closure periods and between the full-closure and gradual-normalization periods, whereas the difference between the partial-closure and gradual-normalization periods was not statistically significant. The corresponding z statistics, Bonferroni-adjusted p-values, and statistical decisions are reported in Table 8. The distributions of the estimated transmission rates across the three intervention groups are further illustrated using box plots in Figure 5.

Table 8. Dunn's post-hoc pairwise comparisons of the estimated transmission rates across intervention periods.

Pairwise comparison	Mean-rank difference	z	Raw p-value	Bonferroni-adjusted p-value	Decision
Full closure vs. Partial closure	−26.034	−3.438	< 0.001	0.002	Reject H_0
Full closure vs. Gradual normalization	−18.160	−3.236	0.001	0.004	Reject H_0
Partial closure vs. Gradual normalization	7.874	1.216	0.224	0.672	Fail to reject H_0

Note: Bonferroni correction was applied to the three pairwise comparisons. The family-wise significance level was $\alpha = 0.05$, yielding an adjusted significance level of $\alpha_{\text{adj}} = 0.0167$. For the two-sided comparisons, the corresponding critical value was $|z| = 2.394$.

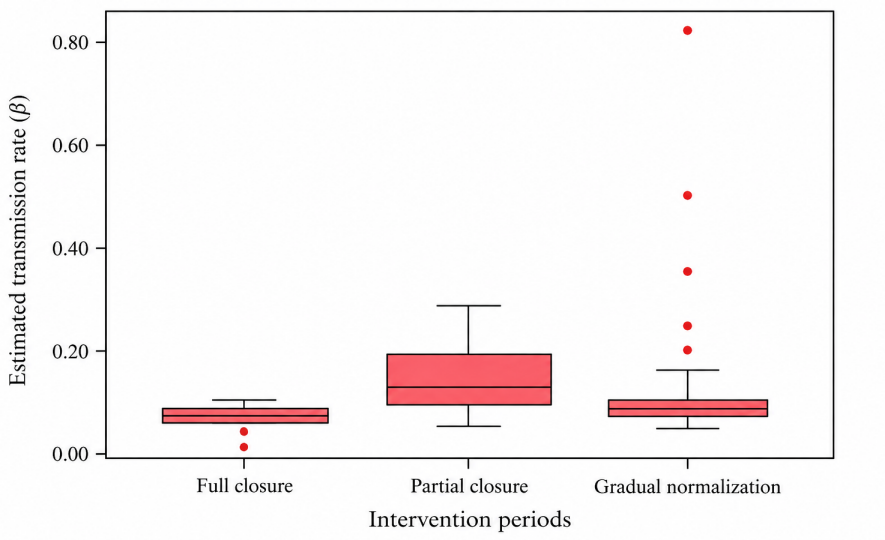


Figure 5. Box plots of the estimated transmission rates across the intervention groups.

Figure 5 provides a graphical comparison of the distributions of the estimated transmission rates across the three intervention groups. The box plots illustrate differences in the location and variability of the transmission-rate estimates among the full-closure, partial-closure, and gradual-normalization periods. In particular, the full-closure group generally exhibits lower transmission-rate estimates than the other two groups, whereas greater variability is observed during the partial-closure period. These graphical patterns are consistent with the Kruskal–Wallis and Dunn's post-hoc results reported above;

however, the statistical significance of the between-group differences is determined by the inferential tests rather than by visual inspection of the box plots.

To assess the robustness of the statistical findings with respect to the assumed recovery rate, a sensitivity analysis was performed using $\gamma = 1/10$ and $\gamma = 1/20$ day^{-1}, in addition to the primary value of $\gamma = 1/14$ day^{-1}. The results are presented in Table 9.

Table 9. Sensitivity analysis of the intervention-period comparisons under alternative recovery-rate assumptions.

γ	$H(2)$	p	Full–Partial adj. p	Full–Gradual adj. p	Partial–Gradual adj. p
1/10	14.353	0.001	0.002	0.004	0.672
1/14	14.353	0.001	0.002	0.004	0.672
1/20	14.353	0.001	0.002	0.004	0.672

Note: Dunn's pairwise comparisons were adjusted using the Bonferroni correction ($\alpha_{\text{adj}} = 0.0167$). The primary analysis was based on $\gamma = 1/14$ day^{-1}.

A consistent inferential pattern was observed across the three recovery-rate assumptions. Because the segment-specific transmission-rate estimates were obtained as $\widehat{\beta}_j = \widehat{b}_j + \gamma$, changing γ while retaining the same segment-specific slope estimates $\widehat{b}_j$ shifts all transmission-rate estimates by the same constant. Consequently, the rank ordering of the estimated transmission rates remains unchanged. Since the Kruskal–Wallis and Dunn procedures are rank-based, their test statistics and pairwise comparison results are identical across the examined values of γ.

For $\gamma = 1/10$, $1/14$, and $1/20$ day^{-1}, the Kruskal–Wallis test yielded $H(2) = 14.353$ with $p = 0.001$. Dunn's post-hoc comparisons with Bonferroni correction showed statistically significant differences between the full-closure and partial-closure periods and between the full-closure and gradual-normalization periods, whereas the difference between the partial-closure and gradual-normalization periods was not statistically significant. Thus, although the numerical values of the estimated transmission rates shift according to the assumed recovery rate, the inferential conclusions regarding the intervention-period comparisons remain unchanged.

To further assess the robustness of these findings, an additional sensitivity analysis was conducted by excluding the negative transmission-rate estimate ($\widehat{\beta} = -0.0200$). The Kruskal–Wallis statistic decreased from $H(2) = 14.353$ ($p = 0.001$, $n = 60$) to $H(2) = 12.572$ ($p = 0.002$, $n = 59$). Dunn's post-hoc comparisons with Bonferroni correction continued to show statistically significant differences between the full-closure and partial-closure periods (adjusted $p = 0.003$) and between the full-closure and gradual-normalization periods (adjusted $p = 0.009$). In contrast, the difference between the partial-closure and gradual-normalization periods remained statistically non-significant (adjusted $p = 0.651$). Although excluding the negative estimate reduced the Kruskal–Wallis statistic and slightly changed the adjusted p-values, the overall statistical significance and the pattern of pairwise differences remained unchanged. These findings indicate that retaining the negative estimate did not alter the principal inferential conclusions.

Based on the estimated transmission rates, the normalized SIR model using the representative full-closure transmission rate $\beta = 0.0654$, corresponding to the median of the transmission-rate estimates obtained for the full-closure segments, and $\gamma = 1/14$ day^{-1} is given by

$$
\begin{aligned}
s'(t) &= -0.0654\, s(t)i(t),\\
i'(t) &= 0.0654\, s(t)i(t) - \frac{1}{14}i(t),\\
r'(t) &= \frac{1}{14}i(t).
\end{aligned}
$$

Since no statistically significant difference was found between the partial-closure and gradual-normalization periods, the transmission-rate estimates from these two groups were combined for the model representation. The median of the combined transmission-rate estimates was $\beta = 0.0763$, which was used as the representative transmission rate. The normalized SIR system is therefore given by

$$
\begin{aligned}
s'(t) &= -0.0763\, s(t)i(t),\\
i'(t) &= 0.0763\, s(t)i(t) - \frac{1}{14}i(t),\\
r'(t) &= \frac{1}{14}i(t).
\end{aligned}
$$

For comparison purposes, an additional counterfactual scenario was considered using $\beta = 0.5684$. This value corresponds to the transmission-rate estimate obtained for the March 11–15, 2020 segment, which was classified as a no-intervention period in the present study. Although $\beta = 0.5684$ was empirically estimated from this segment, its use as a constant transmission rate over the simulated period represents a hypothetical counterfactual scenario rather than an observed epidemic trajectory. The scenario was therefore used as a reference for illustrating model behavior under the transmission conditions represented by this early no-intervention segment. The corresponding normalized SIR system is

$$
\begin{aligned}
s'(t) &= -0.5684\, s(t)i(t),\\
i'(t) &= 0.5684\, s(t)i(t) - \frac{1}{14}i(t),\\
r'(t) &= \frac{1}{14}i(t).
\end{aligned}
$$

To illustrate the potential effect of the transmission rate associated with the full-closure periods, a hypothetical scenario was constructed using $\beta = 0.0654$, which represents the median transmission rate estimated for the full-closure segments. The recovery rate was fixed at $\gamma = 1/14$ day^{-1}. The simulation was initialized on 27 March 2020 using $S(0) = 81{,}994{,}302$, $I(0) = 5{,}564$, and $R(0) = 134$. The model was solved in normalized form, and the infected proportion was subsequently converted to the corresponding number of infected individuals using the total population $N = 82{,}000{,}000$.

Figure 6 compares the observed active-case trajectory with the hypothetical trajectory obtained by imposing the representative full-closure transmission rate throughout the 50-day simulation period. Under this scenario, the number of infected individuals decreases slightly from 5,564 at the initial time to approximately 5,219 on day 50, whereas the observed active-case trajectory increases substantially over the same period. This comparison should therefore be interpreted as a counterfactual model-based illustration of the epidemic trajectory associated with the lower full-closure transmission rate, rather than as a fitted prediction or a causal estimate of what would necessarily have occurred under full closure.

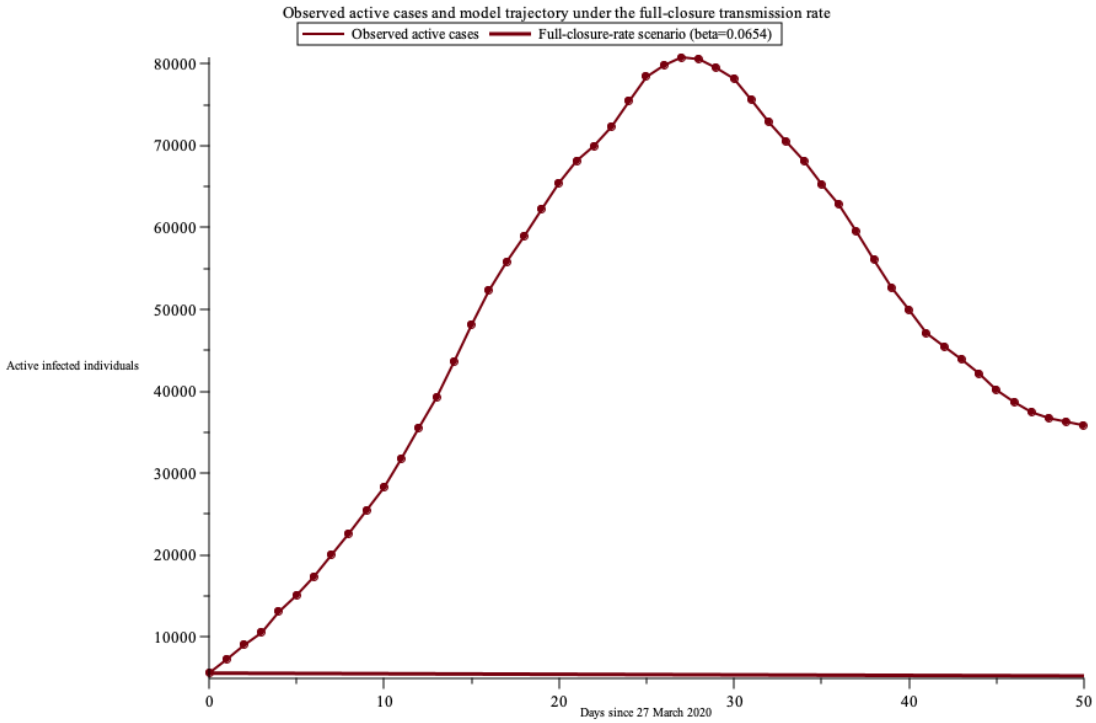


Figure 6. Observed active cases and the hypothetical epidemic trajectory obtained under the representative full-closure transmission rate $\beta = 0.0654$ with $\gamma = 1/14$. The simulation starts on 27 March 2020 and covers a 50-day period.

4. Conclusions

This study investigated temporal changes in COVID-19 transmission dynamics in Türkiye by combining a normalized dynamic SIR model with change-point and non-parametric statistical analyses. In contrast to a conventional SIR formulation with a constant transmission parameter, the recovery rate was set to $\gamma = 1/14$ day^{-1} in the primary analysis, while the transmission rate β was allowed to vary across the periods identified during the course of the epidemic. Change-point analysis based on the CUSUM approach and bootstrap resampling was used to identify structural changes in the case series, and transmission rates were subsequently estimated for the resulting periods and examined in relation to the government intervention periods considered in the study.

The distributions of the estimated transmission rates differed across the full-closure, partial-closure, and gradual-normalization periods. Since the transmission-rate data did not satisfy the normality assumption, the intervention periods were compared using the Kruskal–Wallis test. The analysis indicated an overall statistically significant difference among the three intervention groups ($H(2) = 14.353$, $p = 0.001$). Subsequent pairwise comparisons using Dunn's post-hoc procedure with Bonferroni correction indicated significant differences between full closure and partial closure and between full closure and gradual normalization, whereas the difference between partial closure and gradual normalization was not statistically significant. These inferential conclusions remained unchanged in the sensitivity analyses conducted using $\gamma = 1/10$ and $\gamma = 1/20$ day^{-1} relative to the primary $\gamma = 1/14$ day^{-1} specification, indicating that the inferential pattern was robust across the

examined recovery-rate assumptions.

These results demonstrate that the estimated transmission rates varied across intervention periods; however, they should be interpreted as statistical associations within the modeling framework rather than as direct evidence of a causal effect of the interventions. Overall, the findings illustrate the potential of combining a normalized dynamic SIR framework with change-point detection and non-parametric statistical analysis to characterize temporal variation in epidemic transmission. The model-based comparisons also provide a framework for examining epidemic trajectories under different transmission-rate settings. In particular, the transmission-rate value used in the additional scenario, $\beta = 0.5684$, was estimated from the March 11–15, 2020 segment classified as a no-intervention period in the present study; however, its use as a constant transmission rate over the simulated period represents a hypothetical counterfactual comparison rather than an observed epidemic trajectory. Accordingly, the results are intended to support the quantitative assessment of transmission dynamics and should not be interpreted as definitive predictions of the outcomes that would have occurred under alternative intervention policies.

4.1. Limitations

Several limitations of the present study should be acknowledged. First, the normalized SIR model assumes homogeneous mixing of the population and does not explicitly account for heterogeneity in age, risk level, contact patterns, or other demographic characteristics. The model also does not incorporate natural births and deaths or distinguish asymptomatic and unreported infections from reported cases. Consequently, the observed case data may not fully represent the actual number of infections in the population. In addition, the primary analysis assumed a recovery rate of $\gamma = 1/14$ day^{-1}, corresponding to an assumed mean residence/recovery time of 14 days in the infectious compartment. This assumption simplifies possible temporal and individual variation in the recovery process. Although the sensitivity analysis using alternative recovery-rate assumptions yielded the same inferential conclusions regarding the intervention-period comparisons, uncertainty associated with the specification of γ remains a limitation of the SIR model.

A further limitation concerns the unconstrained segment-wise estimation of the transmission rate. For one rapidly declining segment, the log-linear OLS procedure produced a negative estimate of $\widehat{\beta} = -0.0200$, which has no direct biological interpretation as a transmission rate and instead reflects the limitations of the local approximation used for parameter estimation. This estimate was retained in the primary statistical analysis to maintain consistency with the unconstrained estimation procedure and to avoid selectively excluding an observation or imposing an arbitrary truncation at zero. Although retaining this extreme low-ranked observation may influence rank-based statistical comparisons, the additional sensitivity analysis performed after its exclusion showed that the overall statistical significance and the significance pattern of the Dunn–Bonferroni pairwise comparisons remained unchanged. Nevertheless, the occurrence of a negative estimate highlights the limitations of unconstrained parameter estimation and the need for caution when interpreting segment-specific transmission rates.

An additional limitation concerns the use of daily reported new COVID-19 cases in the segment-wise log-linear estimation. These observations represent incident cases rather than the number of individuals currently in the infectious compartment of the SIR model. Their use as a proxy for local infected-state dynamics relies on an empirical approximation and may be affected by reporting delays,

testing practices, and changes in case ascertainment. Consequently, the resulting segment-specific transmission-rate estimates should be interpreted as model-dependent approximations rather than exact measurements of the underlying transmission parameter.

Furthermore, the association between detected change points and government intervention periods should be interpreted cautiously. Epidemic transmission may be influenced simultaneously by behavioral changes, testing practices, reporting procedures, population mobility, vaccination, emerging variants, and other time-dependent factors that are not explicitly represented in the present model. Therefore, although statistically significant differences in the estimated transmission rates were identified across the intervention periods, these differences cannot by themselves establish a causal effect of a particular government measure. These limitations should be considered when generalizing the findings to other populations, epidemic periods, or public-health policy settings.

Author contributions

Serpil Ünal: Conceptualization, methodology, formal analysis, data curation (conceptualization and design of the intervention-period comparison, development of the statistical comparison methodology, selection and application of statistical tests, collaborative classification of intervention periods, and interpretation of statistical findings); Elçin Çelik: Methodology, formal analysis, software, data curation (contribution to the mathematical and computational analyses, development of Maple and MATLAB codes, and collaborative classification of intervention periods); Deniz Uçar: Conceptualization, methodology, formal analysis (conceptualization, development, and formulation of the mathematical model and contribution to the mathematical analysis). All authors have read and approved the final version of the manuscript for publication.

Use of Generative-AI tools declaration

During the preparation and proofreading of this manuscript, the authors used ChatGPT (OpenAI) to assist with language editing and the conversion of existing tables into LaTeX format. The authors reviewed and verified all AI-assisted revisions and take full responsibility for the content of the manuscript.

Data availability

The datasets analyzed in the present study are publicly available from the Ministry of Health of the Republic of Türkiye COVID-19 Information Platform: https://covid19.saglik.gov.tr/TR-66935/genel-koronavirus-tablosu.html.

Conflict of interest

The authors declare that they have no conflicts of interest.

References

1. J. M. Last, *A dictionary of epidemiology*, 2 Eds., Oxford University Press, 1988.

2. W. O. Kermack, A. G. McKendrick, A contribution to the mathematical theory of epidemics, *Proc. R. Soc. Lond. A*, **115** (1927), 700–721. http://dx.doi.org/10.1098/rspa.1927.0118
3. W. O. Kermack, A. G. McKendrick, Contributions to the mathematical theory of epidemics. II. The problem of endemicity, *Proc. Roy. Soc. Lond. A*, **138** (1932), 55–83. http://dx.doi.org/10.1098/rspa.1932.0171
4. W. O. Kermack, A. G. McKendrick, Contributions to the mathematical theory of epidemics. III. Further studies of the problem of endemicity, *Proc. Roy. Soc. Lond. A*, **141** (1933), 94–122. http://dx.doi.org/10.1098/rspa.1933.0106
5. F. C. Hoppensteadt, *Mathematical methods of population biology*, Cambridge: Cambridge University Press, 2010. http://dx.doi.org/10.1017/CBO9780511624087
6. F. Shakeri, M. Dehghan, Solution of a model describing biological species living together using the variational iteration method, *Math. Comput. Model.*, **48** (2008), 685–699. https://dx.doi.org/10.1016/j.mcm.2007.11.012
7. F. Shakeri, M. Dehghan, Solution of delay differential equations via a homotopy perturbation method, *Math. Comput. Model.*, **48** (2008), 486–498. http://dx.doi.org/10.1016/j.mcm.2007.09.016
8. F. Shakeri, M. Dehghan, Application of the decomposition method of Adomian for solving the pantograph equation of order *m*, *Z. Naturforsch. A*, **65** (2010), 453–460. http://dx.doi.org/10.1515/zna-2010-0510
9. D. J. Evans, K. R. Raslan, The Adomian decomposition method for solving delay differential equation, *Int. J. Comput. Math.*, **82** (2005), 49–54. http://dx.doi.org/10.1080/00207160412331286815
10. A. Saadatmandi, M. Dehghan, Variational iteration method for solving a generalized pantograph equation, *Comput. Math. Appl.*, **58** (2009), 2190–2196. http://dx.doi.org/10.1016/j.camwa.2009.03.017
11. F. S. Akinboro, S. Alao, F. O. Akinpelu, Numerical solution of SIR model using differential transformation method and variational iteration method, *Gen. Math. Notes*, **22** (2014), 82–92.
12. D. Uçar, E. Çelik, Analysis of COVID 19 disease with SIR model and Taylor matrix method, *AIMS Math.*, **7** (2022), 11188–11200. http://dx.doi.org/10.3934/math.2022626
13. B. Shulgin, L. Stone, Z. Agur, Pulse vaccination strategy in the SIR epidemic model, *Bull. Math. Biol.*, **60** (1998), 1123–1148. http://dx.doi.org/10.1016/S0092-8240(98)90005-2
14. M. C. Schuette, H. W. Hethcote, Modeling of the effects of varicella vaccination programs on the incidence of chickenpox and shingles, *Bull. Math. Biol.*, **61** (1999), 1031–1064. http://dx.doi.org/10.1006/bulm.1999.0126
15. D. J. Daley, J. Gani, *Epidemic modelling: An introduction*, Cambridge: Cambridge University Press, 2009. http://dx.doi.org/10.1017/CBO9780511608834
16. M. Iannelli, The mathematical modeling of epidemics, In: *Summer school on mathematical models in life science: Theory and simulation*, 2005.
17. M. Rafei, D. Ganji, H. Daniali, Solution of the epidemic model by homotopy perturbation method, *Appl. Math. Comput.*, **187** (2007), 1056–1062. http://dx.doi.org/10.1016/j.amc.2006.09.019

18. S. Ahmetolan, A. H. Bilge, A. Demirci, A. Peker-Dobie, O. Ergonul, What can we estimate from fatality and infectious case data using the Susceptible-Infected-Removed (SIR) model? A case study of COVID-19 pandemic, *Front. Med.*, **7** (2020), 556366. http://dx.doi.org/10.3389/fmed.2020.556366

19. U. Nguemdjo, F. Meno, A. Dongfack, B. Ventelou, Simulating the progression of the COVID-19 disease in Cameroon using SIR models, *PLoS ONE*, **15** (2020), e0237832. http://dx.doi.org/10.1371/journal.pone.0237832

20. E. B. Postnikov, Estimation of COVID-19 dynamics "On a back-of-envelope": Does the simplest SIR model provide quantitative parameters and predictions?, *Chaos Soliton. Fract.*, **135** (2020), 109841. http://dx.doi.org/10.1016/j.chaos.2020.109841

21. N. R. Record, A. Pershing, A note on the effects of epidemic forecasts on epidemic dynamics, *PeerJ*, **8** (2020), e9649. http://dx.doi.org/10.7717/peerj.9649

22. N. S. Barlow, S. J. Weinstein, Accurate closed-form solution of the SIR epidemic model, *Physica D*, **408** (2020), 132540. http://dx.doi.org/10.1016/j.physd.2020.132540

23. N. A. Kudryashov, M. A. Chmykhov, M. Vigdorowitsch, Analytical features of the SIR model and their applications to COVID-19, *Appl. Math. Model.*, **90** (2021), 466–473. http://dx.doi.org/10.1016/j.apm.2020.08.057

24. N. A. Kudryashov, M. A. Chmykhov, M. Vigdorowitsch, An estimative (warning) model for recognition of pandemic nature of virus infections, *Int. J. Nonlinear Sci. Numer. Simul.*, **24** (2023), 213–226. http://dx.doi.org/10.1515/ijnsns-2020-0154

25. A. Spannaus, T. Papamarkou, S. Erwin, J. B. Christian, Inferring the spread of COVID-19: The role of time-varying reporting rate in epidemiological modelling, *Sci. Rep.*, **12** (2022), 10761. https://doi.org/10.1038/s41598-022-14979-0

26. D. A. Buch, J. E. Johndrow, D. B. Dunson, Explaining transmission rate variations and forecasting epidemic spread in multiple regions with a semiparametric mixed effects SIR model, *Biometrics*, **79** (2023), 2987–2997. https://doi.org/10.1111/biom.13901

27. R. Mbuvha, T. Marwala, Bayesian inference of COVID-19 spreading rates in South Africa, *PLoS ONE*, **15** (2020), e0237126. https://doi.org/10.1371/journal.pone.0237126

28. N. Güzey, Türkiye'deki COVID-19 yayılımının SIR temelli modellenmesinde RSS yöntemi ile parametre kestirimi, *GÜFBED*, **11** (2021), 956–963. https://doi.org/10.17714/gumusfenbil.757291

29. H. Sjödin, A. Wilder-Smith, S. Osman, Z. Farooq, J. Rocklöv, Only strict quarantine measures can curb the coronavirus disease (COVID-19) outbreak in Italy, 2020, *Eurosurveillance*, **25** (2020), 2000280. http://dx.doi.org/10.2807/1560-7917.ES.2020.25.13.2000280

30. A. S. Alshomrani, M. Z. Ullah, D. Baleanu, Caputo SIR model for COVID-19 under optimized fractional order, *Adv. Differ. Equ.*, **2021** (2021), 185. http://dx.doi.org/10.1186/s13662-021-03345-5

31. M. Sezer, A method for the approximate solution of the second-order linear differential equations in terms of Taylor polynomials, *Int. J. Math. Educ. Sci. Technol.*, **27** (1996), 821–834. http://dx.doi.org/10.1080/0020739960270606

32. M. Sezer, A. Karamete, M. Gülsu, Taylor polynomial solutions of systems of linear differential equations with variable coefficients, *Int. J. Comput. Math.*, **82** (2005), 755–764. http://dx.doi.org/10.1080/00207160512331323336

33. W. A. Taylor, *Change-point analysis: A powerful new tool for detecting changes*, Taylor Enterprises, Inc., 2012.

34. G. Duan, H. Gong, B. Chen, X. Li, X. Pan, M. Shi, et al., Spatiotemporal heterogeneity of land subsidence in Beijing, *Sci. Rep.*, **12** (2022), 15120. https://doi.org/10.1038/s41598-022-16674-6

35. W. A. Taylor, Change-point analyzer: Advanced options dialog box, Taylor Enterprises, Inc. Available from: `https://variation.com/wp-content/change-point_analyzer_help/hs50.htm`

36. A. Dinno, Nonparametric pairwise multiple comparisons in independent groups using Dunn's test, *Stata J.*, **15** (2015), 292–300. https://doi.org/10.1177/1536867X1501500117

37. S. Genç, M. I. Soysal, Parametrik ve parametrik olmayan çoklu karşılaştırma testleri, *Black Sea J. Eng. Sci.*, **1** (2018), 18–27.

38. Republic of Türkiye Ministry of Health, COVID-19 general coronavirus table, Available from: `https://covid19.saglik.gov.tr/TR-66935/genel-koronavirus-tablosu.html`

39. J. Hu, W. Liang, H. Dai, Y. Bao, Efficient empirical likelihood inference for recovery rate of COVID-19 under double-censoring, *J. Stat. Plann. Inference*, **221** (2022), 172–187. https://doi.org/10.1016/j.jspi.2022.04.005

Supplementary

Supplementary Table S1 presents the detected change points, bootstrap confidence levels, corresponding intervention dates, temporal differences, intervention categories, and estimated transmission rates.

Table S1. Detected change points and their correspondence with government intervention periods.

Detected change-point date	Bootstrap confidence level (%)	Corresponding intervention date	Temporal difference (days)	Intervention category	Estimated β
March 15, 2020	81.80	March 16, 2020	+1	Partial Closure	0.6564
March 18, 2020	99.50	March 16, 2020	−2	Partial Closure	0.1700
March 24, 2020	99.40	March 16, 2020	−8	Partial Closure	0.2520
March 30, 2020	80.60	March 16, 2020	−14	Partial Closure	0.1218
April 6, 2020	99.90	No intervention within ±14 days	—	Partial Closure	0.0731
April 21, 2020	99.90	April 23, 2020	+2	Full Closure	0.0434
April 30, 2020	99.00	May 1, 2020	+1	Full Closure	0.0699
May 8, 2020	99.70	May 4, 2020	−4	Gradual Normalization	0.0789
May 17, 2020	99.90	May 16, 2020	−1	Full Closure	0.0771
May 29, 2020	99.70	May 27, 2020	−2	Gradual Normalization	0.0818
June 11, 2020	99.80	No intervention within ±14 days	—	Gradual Normalization	0.0640
July 5, 2020	87.90	No intervention within ±14 days	—	Gradual Normalization	0.0621

Continued on next page

Table S1 (continued)

Detected change-point date	Bootstrap confidence level (%)	Corresponding intervention date	Temporal difference (days)	Intervention category	Estimated β
July 14, 2020	87.00	No intervention within ±14 days	—	Gradual Normalization	0.0700
July 27, 2020	99.60	No intervention within ±14 days	—	Gradual Normalization	0.0796
August 3, 2020	99.80	No intervention within ±14 days	—	Gradual Normalization	0.0782
August 23, 2020	99.70	No intervention within ±14 days	—	Gradual Normalization	0.0842
September 1, 2020	99.20	No intervention within ±14 days	—	Gradual Normalization	0.0733
September 25, 2020	99.80	No intervention within ±14 days	—	Gradual Normalization	0.0691
October 4, 2020	99.40	No intervention within ±14 days	—	Gradual Normalization	0.0809
October 17, 2020	100.0	No intervention within ±14 days	—	Gradual Normalization	0.0871
October 25, 2020	96.40	No intervention within ±14 days	—	Gradual Normalization	0.0675
November 1, 2020	88.60	No intervention within ±14 days	—	Gradual Normalization	0.0899
November 12, 2020	100.0	No intervention within ±14 days	—	Gradual Normalization	0.1572
November 24, 2020	100.0	No intervention within ±14 days	—	Gradual Normalization	0.0543
December 1, 2020	96.30	December 11, 2020	+10	Gradual Normalization	0.3761
December 11, 2020	99.50	December 11, 2020	0	Full Closure	0.0621
December 18, 2020	100.0	December 11, 2020	−7	Full Closure	0.0394
December 24, 2020	97.90	December 11, 2020	−13	Full Closure	0.0605
December 30, 2020	100.0	No intervention within ±14 days	—	Full Closure	0.0696
January 8, 2021	96.30	No intervention within ±14 days	—	Full Closure	0.0654
January 14, 2021	100.0	No intervention within ±14 days	—	Full Closure	0.0697
January 31, 2021	100.0	No intervention within ±14 days	—	Full Closure	0.0665
February 21, 2021	98.40	March 1, 2021	+8	Partial Closure	0.0750
February 28, 2021	100.0	March 1, 2021	+1	Partial Closure	0.0987
March 9, 2021	97.40	March 1, 2021	−8	Gradual Normalization	0.1117
March 18, 2021	100.0	No intervention within ±14 days	—	Gradual Normalization	0.1224
March 23, 2021	95.70	No intervention within ±14 days	—	Gradual Normalization	0.0924
March 25, 2021	94.90	No intervention within ±14 days	—	Gradual Normalization	0.1164
April 1, 2021	100.0	April 14, 2021	+13	Gradual Normalization	0.0644
April 5, 2021	97.40	April 14, 2021	+9	Gradual Normalization	0.0705
April 11, 2021	99.40	April 14, 2021	+3	Partial Closure	0.0628
April 23, 2021	100.0	April 14, 2021	−9	Partial Closure	0.0685
April 29, 2021	99.20	April 29, 2021	0	Full Closure	0.0044
May 5, 2021	100.0	April 29, 2021	−6	Full Closure	−0.0200
May 12, 2021	98.50	April 29, 2021	−13	Full Closure	0.0707
May 19, 2021	99.20	No intervention within ±14 days	—	Gradual Normalization	0.0596
May 27, 2021	100.0	No intervention within ±14 days	—	Gradual Normalization	0.0500
June 3, 2021	97.40	No intervention within ±14 days	—	Gradual Normalization	0.0792

Continued on next page

Table S1 (continued)

Detected change-point date	Bootstrap confidence level (%)	Corresponding intervention date	Temporal difference (days)	Intervention category	Estimated β
June 12, 2021	100.0	No intervention within ±14 days	—	Gradual Normalization	0.0742
June 25, 2021	97.80	July 1, 2021	+6	Gradual Normalization	0.0763
July 13, 2021	100.0	July 1, 2021	−12	Gradual Normalization	0.1066
July 22, 2021	95.40	No intervention within ±14 days	—	Gradual Normalization	0.2104
July 26, 2021	100.0	No intervention within ±14 days	—	Gradual Normalization	0.0832
August 2, 2021	97.70	No intervention within ±14 days	—	Gradual Normalization	0.0682
August 12, 2021	100.0	No intervention within ±14 days	—	Gradual Normalization	0.0660
August 30, 2021	100.0	No intervention within ±14 days	—	Gradual Normalization	0.0754
September 13, 2021	100.0	No intervention within ±14 days	—	Gradual Normalization	0.0727
October 3, 2021	98.10	No intervention within ±14 days	—	Gradual Normalization	0.0688
October 23, 2021	100.0	No intervention within ±14 days	—	Gradual Normalization	0.0757
November 10, 2021	99.70	No intervention within ±14 days	—	Gradual Normalization	0.0653

Note. Temporal correspondence was assessed using a predefined ±14-day window around each detected change point. The temporal difference equals the intervention date minus the change-point date; positive and negative values indicate that the intervention occurred after and before the change point, respectively. A dash indicates that no documented intervention change occurred within this window. Intervention categories refer to the periods associated with the estimated β segments and were assigned independently of this temporal matching. Temporal proximity does not imply causation. Estimates were obtained using $\gamma = 1/14$ day^{-1}. The negative $\widehat{\beta}$ estimate reflects unconstrained estimation and has no biological interpretation as a transmission rate.



AIMS Press

© 2026 the Author(s), licensee AIMS Press. This is an open access article distributed under the terms of the Creative Commons Attribution License (https://creativecommons.org/licenses/by/4.0)